Demonstration of Flexible Hybrid Sealants by Calcium Corrosion Testing for Organic Photovoltaic Application

THESIS

Presented in Partial Fulfillment of the Requirements for the Degree Master of Science in the Graduate School of The Ohio State University

By

Minjae Kim

Graduate Program in Electrical and Computer Engineering

The Ohio State University

2017

Master's Examination Committee:

Prof. Paul R. Berger, Advisor

Prof. Betty L. Anderson

Abstract

Technical and economic viability of photovoltaic (PV) technology are governed by three parameters: efficiency, cost and lifetime. Since its inception, having benefited from inexpensive mass production capability by roll-to-roll processing, the main driver in organic photovoltaics (OPV) research has been towards achieving high efficiency. Continued effort was fructified with achievement surpassing 10% OPV efficiency, long considered a break-even point for commercial viability. Shifting research focus towards extended lifetime was a next logical step. Increased lifetime of OPV by reliable encapsulation enhances technical feasibility and economic viability. So far, focus has been given on encapsulation barrier films, and little effort has been made on sealants themselves or sealants that have dual functionality as encapsulants; of this limited effort, the testing of existing commercial sealants is the general trend.

Requirements of sealants for OPV encapsulation include compatibility with low-cost and low-temperature OPV processing, lightness, flexibility, transparency, as well as thermal and UV stability. Hybrid sealants combine the advantages of low permeability of inorganic sealants with the flexibility of organic sealants. This thesis is on the demonstration of new flexible hybrid prototype sealants by calcium corrosion testing.

Foremost, electronic properties and historical developments of organic semiconductors are reviewed in Chapter 2. Focus is given to difference between organic

and inorganic semiconductors. Subsequently, we expatiate on photocurrent generation process in OPVs, including generation and diffusion of excitons, followed by dissociation of excitons and collection of charge carriers. Chapter 2 is concluded with OPV economics and lifetime.

In Chapter 3, development and demonstration of sealants are presented. Sealants are screen-printable, flexible and compatible with low-temperature processing of OPVs. Sealing capability of the hybrid sealants was compared with commercial silicone based hybrid sealant, i.e. polydimethylsiloxane (PDMS). Far superior sealing capability, compared to PDMS was demonstrated by calcium corrosion test in ambient air.

Acknowledgments

I would like to express my sincere gratitude to Prof. Paul R. Berger for his motivation, insight and support. His guidance helped me in all the time of research and writing of this thesis.

I would also like to thank my thesis committee Prof. Betty L. Anderson for her insightful comments to ameliorate this thesis.

My sincere thanks also go to Alex Kawczak and Dr. Mike Clingerman for technical discussion and supplying samples. I thank my fellow graduate students whom I worked with, Drs. Woo-Jun Yoon, Si-Young Park, Anisha Ramesh and Tyler Growden, as well as Connor Chambers and Jeremy Guttman.

Vita

2006.....B.S. Electrical and Electronic Engineering, Yonsei University

2008.....M.S. Electrical and Electronic Engineering, Yonsei University

2010 to present .....Graduate Teaching and Research Associate, Department of Electrical and Computer Engineering, The Ohio State University

Publications

1. P. R. Berger and **M. Kim**, "Polymer Solar Cells : P3HT:PCBM and Beyond", submitted per invitation, *Journal of Renewable and Sustainable Energy*

2. S.X. Suleymanov, P. Berger, V.G. Dyskin, M.U. Djanklich, A.G. Bugakov, O.A. Dudko, N.A. Kulagina, **M. Kim**, "Antireflection Composite Coatings for Organic Solar Cells," *Applied Solar Energy*, vol.52, issue 2, pp.157-158, Sep. 2016

3. S.X. Suleymanov, P. Berger, V.G. Dyskin, M.U. Djanklich, A.G. Bugakov, O.A. Dudko, N.A. Kulagina, and **M. Kim**, "Antireflection Coatings Based on Fluoride Formulations for Organic Solar Cells," *Technical Physics Letters*, vol. 42, issue 4, pp.359-361, Apr. 2016

4. D. Cheyns, **M. Kim**, B. Verreet, B. P. Rand, "Accurate Spectral Response Measurements of a Complementary Absorbing Organic Tandem Cell with Fill Factor Exceeding the Subcells," *Applied Physics Letters*, vol. 104, issue 9, 093302, Mar. 2014

5. **M. Kim**, M. Clingerman, A. Kawczak, P. R. Berger, "Demonstration of Hybrid Prototype Sealant for Encapsulating Organic Photovoltaics," *IEEE 38th Photovoltaic Specialists Conference (PVSC)*, Austin, Texas, USA, Jun.2012

6. Y. J. Kim, M. C. Ahn, D. K. Park, **M. J. Kim**, S. E. Yang, T. K. Ko, H. K. Kang, K. W. Nam, J.-H. Kim, J.-B. Song, H. Lee, "Quench and Recovery Test on Stacked YBCO-Coated Conductors by Applying Various Intermediate Inserting Materials," *Japanese Journal of Applied Physics*, vol.48, no.3, issue 1, 033001, Mar. 2009

7. **M. J. Kim**, M. C. Ahn, S. E. Yang, D. K. Park, Y. Kim, C. Lee, B.-Y. Seok, T. K. Ko, "Determination of Maximum Permissible Temperature Rise Considering Repetitive Over-Current Characteristics of YBCO Coated Conductors," *IEEE Transactions on Applied Superconductivity*, vol.18, no.2, pp.660-663, Jul. 2008

8. **M. J. Kim**, S. E. Yang, M. C. Ahn, D. K. Park, Y. Kim, Y. S. Yoon, T. K. Ko, "Short-Circuit Characteristics of Non-Inductive Superconducting Coil Wound With Stainless Steel-Stabilized Coated Conductor in Sub-Cooled Liquid Nitrogen," *Physica C*, Elsevier, vol. 463-465, pp.1181-1187, Oct. 2007

9. M. C. Ahn, D. K. Park, S. E. Yang, **M. J. Kim**, C. Lee, B.-Y. Seok, T. K. Ko, "Basic Design of 22.9kV/630A Resistive Superconducting Fault Current Limiter Using YBCO Coated Conductor," *Physica C*, vol.463-465, pp.1176-1180, Oct. 2007

10. M. C. Ahn, D. K. Park, S. E. Yang, **M. J. Kim**, H. M. Kim, H. Kang, K. Nam, B.-Y. Seok, J.-W. Park, T. K. Ko, "A Study on the Design of the Stabilizer of Coated Conductor for Applying to SFCL," IEEE Transactions on Applied Superconductivity, vol.17, no.2, pp.1855-1858, Jun.2007 (cited by 21)

11. M. C. Ahn, D. K. Park, S. E. Yang, **M. J. Kim**, H. M. Chang, Y. S. Yoon, B.-Y. Seok, J.-W. Park, T. K. Ko, "Recovery Characteristics of Resistive SFCL Wound With YBCO Coated Conductor in a Power System," *IEEE Transactions on Applied Superconductivity*, vol.17, no.2, pp.1859-1862, Jun. 2007

12. S. E. Yang, D. K. Park, M. C. Ahn, Y. S. Kim, **M. J. Kim**, Y. S. Yoon, C. Lee, B.-Y. Seok, T. K. Ko, "Manufacture and Test of the Bifilar Wound Coil Using Coated Conductor with Stainless Steel Stabilizer," *IEEE Transactions on Applied Superconductivity*, vol.17, no.2, pp.1867-1870, Jun. 2007

Fields of Study

Major Field: Electrical and Computer Engineering

Table of Contents

List of Figures

Chapter 1

Introduction

In an effort to forage renewable and affordable energy sources, triggered by depletion of fossil fuels and concerns regarding global warming, harvesting energy from sunlight by using photovoltaic (PV) technology has attracted a surge of interest. PV cells are traditionally classified into three generations. Silicon solar cells dominate the first generation and demonstrate efficiencies ranging between 15-20%. The second generation of PV are the thin film technologies that include amorphous silicon, copper-indium-gallium-diselenide (CIGS) and cadminum telluride (CdTe). All of these technologies are deposited atop substrates, sometimes stainless steel, and their efficiencies range between 10-15%. Organic photovoltaics (OPV) are classified as an emerging PV technology that belongs to the third generation of PV cells. Intrinsic properties of organic photovoltaics have suggested them not only as a promising alternative but also as a tantalizing complement to conventional inorganic photovoltaics. Among various solar technologies, organic photovoltaic technology distinguishes itself as an economically feasible solution owing to its mass production capability by means of low-cost roll-to-roll manufacturing [1], although the high cost of raw materials, like functionalized fullerenes often seems

counter. Furthermore, mechanical flexibility, light weight, and transparency of OPV enable portable, wearable energy source [2] or window tinting applications [3] which cannot be realized by inorganic photovoltaic technology. Thus, their form factor make them more expedient as "point-of-use" compact power sources, often embedded inside society and inside the city, whereas Gen1 and Gen2 technologies are relegated to solar farms outside the city, or on rooftops. By being sui generis in the sense that it is "compatible and competitive" to its inorganic counterparts, organic photovoltaic technology has been a cynosure in the PV community. The number of patent applications in the OPV area for the last three decades seemingly indicates that OPV technology has already advanced into maturity. The technology life cycle (TLC) is often used to identify and evaluate the status of a technology development, predominantly correlated to the number of patent applications over time. [4-7] In general, the normal trend in technology advancement is at first slow, accelerates, reaches a plateau, and then declines. Respectively, the S-shaped TLC curve consists of four main stages: emerging, growth, maturity, and saturation. Figure 1 shows the S-curve of the TLC.

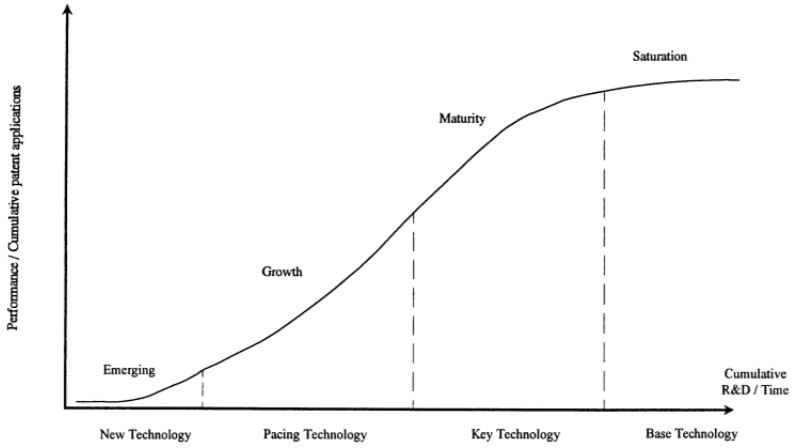

Figure 1. S-Curve of the technology life cycle. Reprinted with permission from Small Business Econ., 9, 361 (1997). Copyright 1997 Kluwer Academic Publishers.

Figure 2 shows the cumulative number of patent applications in the OPV area. To elaborate, the number of patent applications in the area of OPV cells was searched by Cooperative Patent Classification code of OPV cell, i.e. “Y02E 10/549”5 at United States Patent and Trademark Office (USPTO).

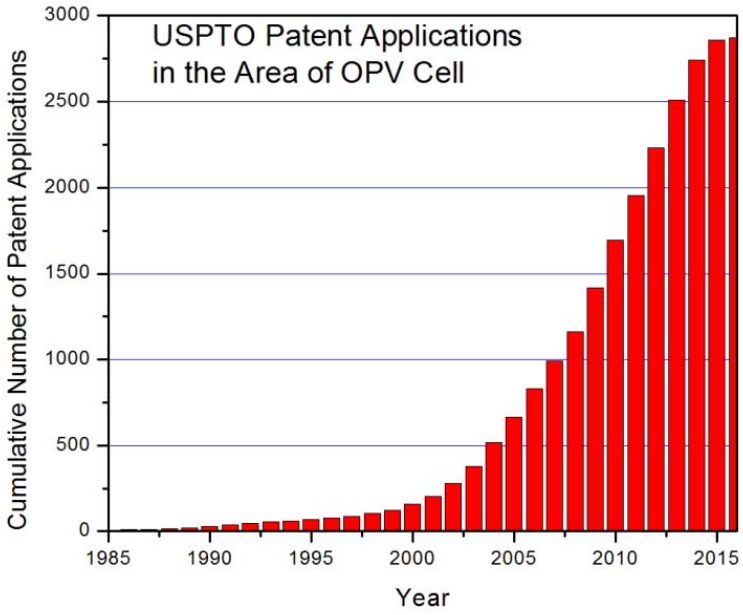

Figure 2. Cumulative number of USPTO patent applications in the area of OPV cells (searched by CPC code of OPV cell. *i.e.* "Y02E 10/549")

As shown in the patent trend, the number of OPV-related patent applications during the nascent stage of OPV development showed slow growth. Subsequently, the number of OPV related patent applications gained considerable momentum from 2000 till 2009, followed by stagnation after 2013. This patent trend, projected into the TLC, indicates that the transition from growth to maturity stage in OPV technology advancement was around 2013. In addition, current OPV technology advancement falls between maturity and saturation stage in the TLC curve, as evidenced by significant drop in the number of patent applications from 2014. Analysis on the trend of patent applications in upcoming years will help better identify and assess the status of OPV technology advancement.

For the last two decades, extensive efforts have been devoted towards research on PSCs, as evidenced by the number of scientific publications in the area [8]. Figure 3 shows the number of scientific publications in the area of PSCs and best record efficiency over time. The number of PSC-related scientific articles published from 1995 to 2016 was searched by the keyword "polymer solar cells" on Institute for Scientific Information's (ISI) Web of Science.

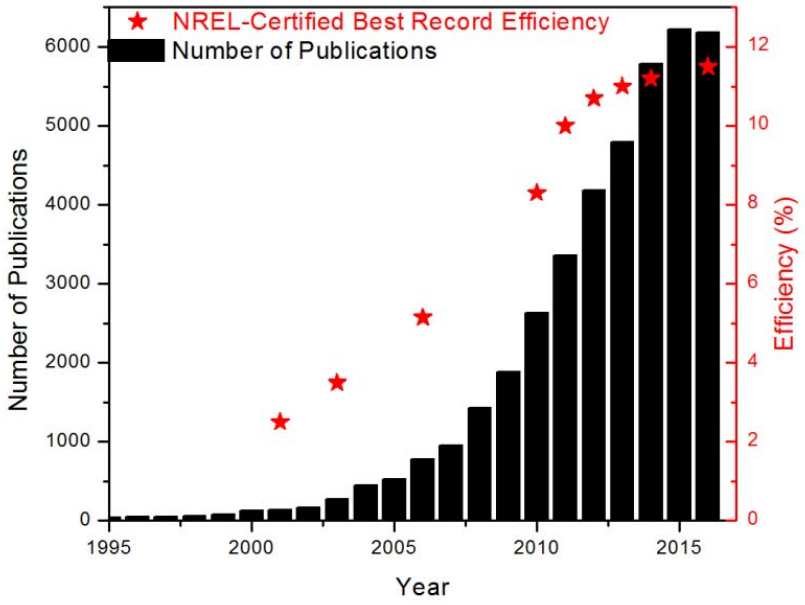

Figure 3. Number of publications in the area of PSCs (left y-axis) and NREL-certified best record efficiency (right y-axis) from 1995 till 2016.

As seen in Figure 3, PSC-related publications are steadily increasing. Notably, the number of publications in the area of PSC doubled every 2-3 years from 1998 to 2012. The best record efficiency data was extracted by cross-examining the best research cell efficiencies published by the National Renewable Energy Laboratory (NREL) and the

solar efficiency table published in Progress in Photovoltaics. [9-20] Both the record efficiency and number of publications exhibit similar trends: accelerated growth from 2001 to 2013, which plateaued, subsequently.

Technical and economic viability of photovoltaic (PV) technology are governed by the triumvirs: efficiency, cost and lifetime. Among various PV technologies, organic photovoltaic (OPV) technology distinguishes itself as a potentially economically feasible solution owing to its mass production capability by means of low-cost roll-to-roll manufacturing [21-23], although the high cost of raw materials, like functionalized fullerenes often seems counter. Since its inception and having benefited from low-cost processing, the main driver in OPV research has been towards the achievement of higher record breaking efficiencies. Through refined device geometry [24-25], tailored synthesis and/or combination of new materials [26-28], and heuristic process optimization [29], the efficiency of OPV cells has climbed to over 10 % [30], which was considered as a break-even point by the National Renewable Energy Laboratory for commercial viability [31] and the highest reasonably achievable number by theoretical predictions [32].

Shifting the focus to OPV lifetime is the next logical step. It is well known that exposure of unprotected OPV cells to ambient air leads to the degradation of photovoltaic performance, which is why OPV cells are generally synthesized inside nitrogen glove-boxes. After fabrication, they are often encapsulated before exposure to ambient air. The most preponderant encapsulation method is by using two barrier films and a sealant; OPV cells are sandwiched between front and back barrier films, whose edges are glued

together by the sealant. Therefore, OPV cells can be protected vertically by barrier films and horizontally by the sealant.

So far, the research focus has been given to the encapsulation barrier films [33], but little strategic effort has been made on the sealant itself; of this limited effort, the testing of existing commercial sealants is the general trend. In this thesis, we report on the development and testing of new flexible hybrid sealants. Our sealants have the major thrusts of OPV devices; they are flexible, compatible with low-cost and low-temperature processing; that is, curable at 130 ^{0}C and screen printable. Their sealing and encapsulating capabilities were demonstrated using the calcium corrosion test in ambient air.

Chapter 2

Polymer:fullerene derivatives bulk-heterojunction solar cells

2.1 Conjugated polymers

Polymers had been regarded strictly as insulators and extensively used in electronics until the discovery of a new class of polymers 40 years ago: conducting polymers. In 1977, Shirakawa, MacDiarmid and Heeger discovered polyacetylene films, when oxidized with chlorine, bromine, or iodine vapor, became 109 times more conductive than they originally were [34], leading to their Noble Prize in 2000. Conjugated polymers, such as polyacetylene, have double bonds separated by single bonds along the carbon-based backbones. This bond alternation opens up the forbidden energy bandgap systemic to semiconductors. Intrinsically, conjugated polymers are insulators or at best weak semiconductors. What makes conjugated polymers conductive is by removing or adding electrons: electrochemical oxidation or reduction, respectively. This redox chemistry is analogous to doping in inorganic semiconductors. By oxidation of conjugated polymers, delocalized electrons are removed from the highest energy pi-bonding orbital, leaving radical cations in which the charge can move along the polymer

chain and also be transferred from one chain to another, thereby enabling conjugated polymers to conduct electricity. Hence, suffice it to say that conductivity of conjugated polymers can be controlled by the degree of doping. The discovery of conducting polymers initially led to research efforts towards conducting properties of polymers for electric wire application. Later, interest has been shifted towards the semiconducting properties of conjugated polymers. Various polymer materials used in PSCs are shown in Figure 4.

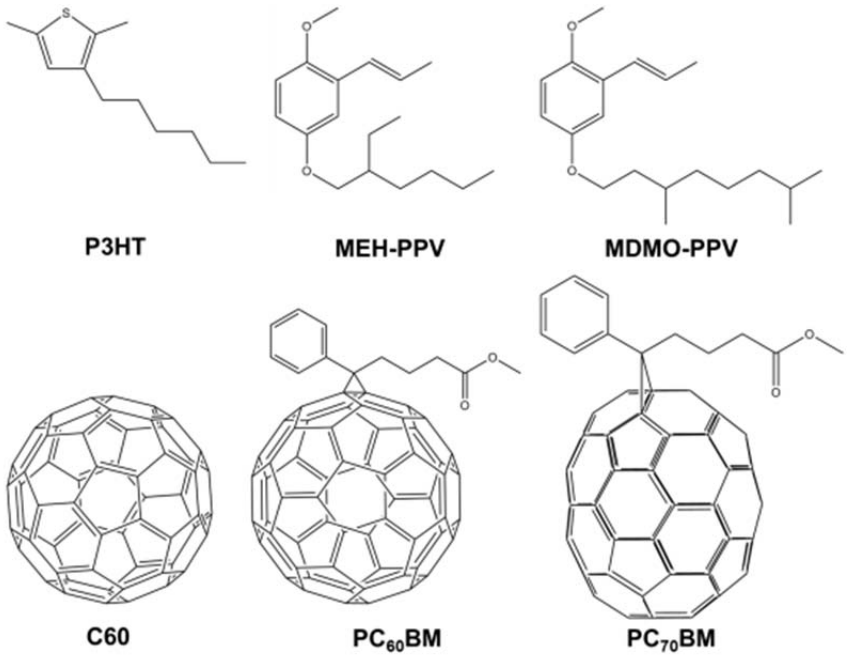

Figure 4. Molecular structures of various donor (top row) and acceptor (bottom row) materials used in PSCs.

One of most important properties of conjugated polymers for the design of PSCs is the bandgap as it controls their electrical and optical characteristics. The bandgap refers to the energy difference between the highest occupied molecular orbital (HOMO) and

lowest unoccupied molecular orbital (LUMO). The HOMO level of organic semiconductors is analogous to the valence band maximum of inorganic semiconductors, whereas the LUMO level of polymer semiconductors is analogous to the conduction band minimum of inorganic semiconductors.

2.2 Photocurrent generation in OPVs

Photocurrent generation in OPVs can be described as a four step process: (i) exciton generation by light absorption; (ii) excitons diffusion; (iii) exciton dissociation; and (iv) carrier collection. Figure 5 shows a schematic illustration of the photocurrent generation process.

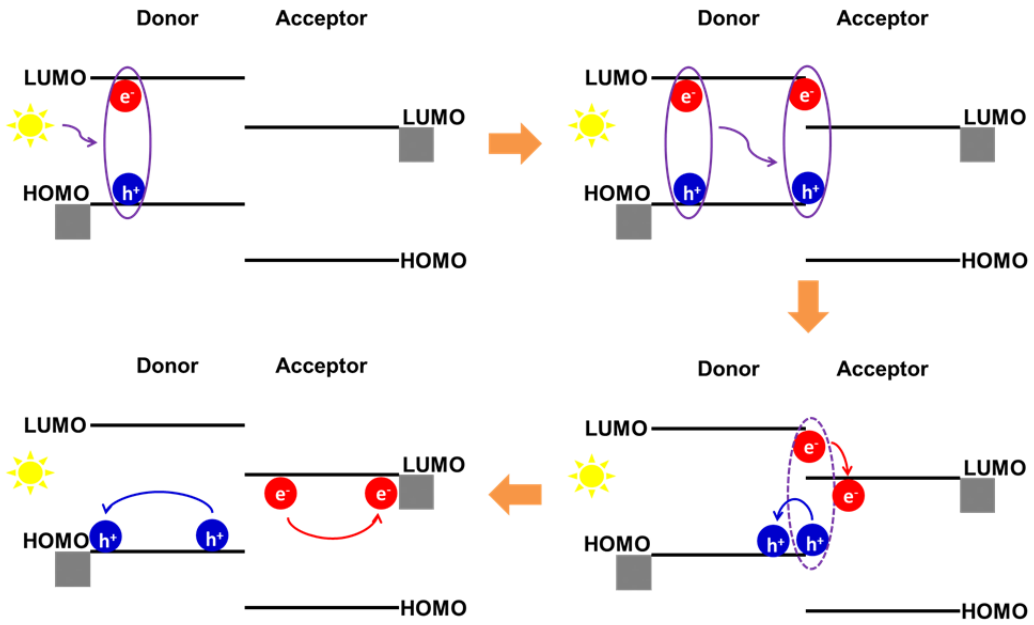

Figure 5. Photocurrent generation process in OPVs: i) exciton generation, ii) exciton diffusion, iii) exciton dissociation and iv) carrier collection, clockwise from top left.

Internal quantum efficiency (IQE) is the ratio of the number of charge carriers collected at the electrodes to the number of incident photons of a given energy. Given the photocurrent generation steps, IQE can be expressed as follows:

$$\eta_{IQE}=\eta_{abs}\,\eta_{diff}\,\eta_{ed}\,\eta_{cc}$$

where η_{abs}, η_{diff}, η_{ed}, and η_{cc} are the photon absorption efficiency, the exciton diffusion efficiency, the exciton dissociation efficiency, and the charge collection efficiency, respectively. External quantum efficiency (EQE), the ratio of the number of charge carriers collected at the electrodes to the number of absorbed photons of a given energy, can be expressed by

$$\eta_{EQE}=(1-R)\,\eta_{abs}\,\eta_{diff}\,\eta_{ed}\,\eta_{cc}$$

where R is the reflectivity of the substrate-air interface.

The fundamental difference between organic and inorganic semiconductors in regards to photocurrent generation in PV cells is their dielectric constants; organic semiconductors typically have low dielectric constant (ε = 2-4) and thus upon absorption of sunlight, a Coulombically bound electron-hole pair, known as an exciton is generated. On the contrary, inorganic semiconductors have high dielectric constants (e.g. $\varepsilon > 10$ for silicon etc.) and hence free electrons and holes are generated [35]. Figure 6 illustrates the binding energy between a photogenerated hole at the origin and an electron at the indicated distance from the hole.

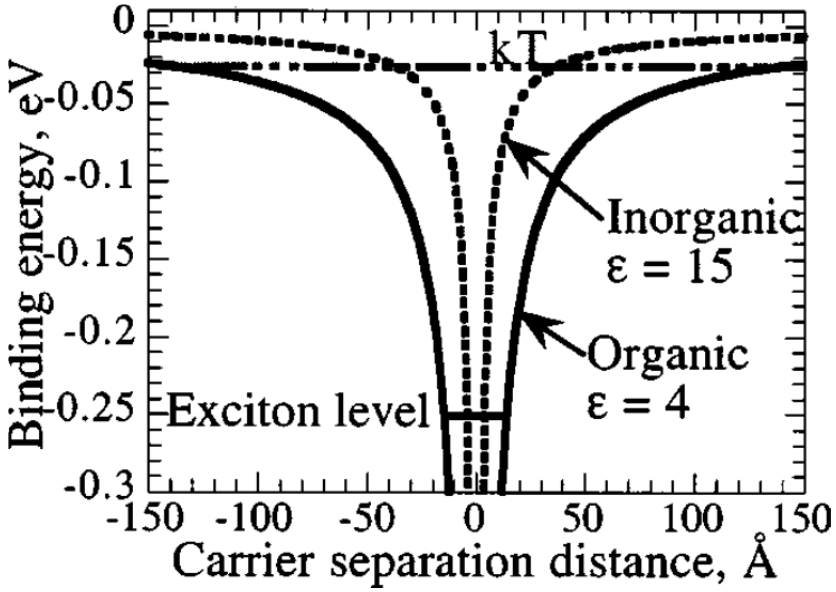

Figure 6. Binding energy between a hole at the origin and an electron at the indicated distance from the hole. Reprinted with permission from J. Appl. Phys., 93, 3605 (2003). Copyright 2003 American Institute of Physics.

Due to Columbic screening differences, excitons in inorganic semiconductors are highly localized with weak binding energies for dissociation and photocurrent collection, whereas the excitons within an organic semiconductor matrix are delocalized over 10 or more bond lengths, with quite significant binding energies required for their dissociation. In addition, the absorption coefficient and carrier mobility in organic semiconductors play important roles in the design of PSCs. Organic semiconductors have much higher extinction, or absorption, coefficients than inorganic semiconductors (~10 times), enabling thinner active region layers for equivalent photon capture. For PSCs, only about 300 nm is thick enough to absorb most incident light as opposed to a few microns for silicon solar cells. However, due to the low carrier mobility, and subsequently short

diffusion length before recombination, of organic semiconductors, about 100 nm is considered as an optimized thickness for PSCs.

Generated excitons are by nature charge neutral and therefore do not drift in an electric field. They will diffuse during their lifetime until they are recombined and/or separated. Their lifetime is in nanoseconds and diffusion length is only about 5-20 nm on average [36]. If an exciton reaches the interface between a donor and acceptor, characterized by the large electronegativity differences between them, by diffusion in its lifetime, it will dissociate into free charge carriers, otherwise it will decay via radiative or non-radiative recombination. Charge carriers in inorganic semiconductors separate when they reach the depletion region. Organic semiconductors require a force larger than the exciton binding energy for exciton dissociation, which is typically 0.3-0.4 eV. [35,37] However, the average thermal energy in the system (kT @ 300 K = 25.9 meV) is much lower than that. Instead, exciton dissociation is driven by the offset in LUMO energies between acceptor and donor, which becomes an OPV efficiency loss in terms of a reduction of its open circuit voltage. Figure 7 shows the band diagram of an OPV cell.

Separated electrons and holes migrate to the cathode and anode, respectively, driven by the work function difference between the two electrodes. In addition, electron and hole mobilities should be balanced to avoid space charge buildup and recombination.

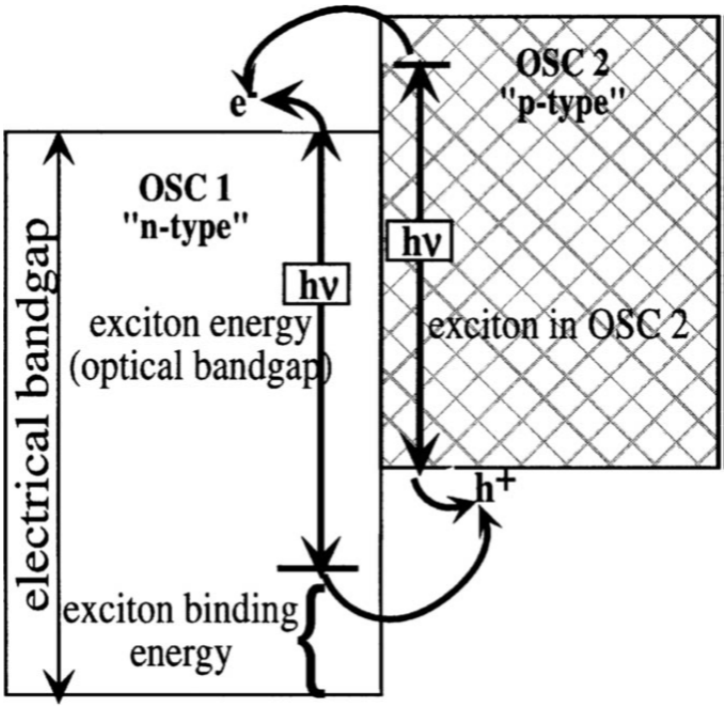

Figure 7. Energy-level diagram of an OPV cell. Reprinted with permission from J. Appl. Phys., 93, 3605 (2003). Copyright 2003 American Institute of Physics.

2.3 History of Organic Photovoltaics

Inchoate efforts towards improving PCE in PSCs focused on device geometry for improved charge separation, selection of materials and process optimization for better light absorption and charge transport. Initial efforts led to the successful bulk heterojunction device geometry, in combination with material combination of poly(2-methoxy-5-(3′,7′-dimethyloctyloxy)-1,4-phenylene vinylene (MDMO-PPV) and phenyl-C61-Butyric-Acid-Methyl Ester (PCBM). Subsequently, interest was shifted to PSCs using the baseline model of poly(3-hexylthiophene-2,5-diyl) (P3HT) interspersed with

PCBM. The P3HT:PCBM had been the "best seller" in PSC research for almost a decade since first reported in 2002 [38,39]. Through nanomorphology control by process optimization, assisted by advances in high resolution scanning probe microscopy techniques, P3HT:PCBM PSC achieved the best NREL-certified record efficiency of 5.4 %. [40]

2.3.1 Device geometry

Device geometry of OPVs evolved from a simple single layer, to a planar heterojunction (PHJ), and finally to the bulk heterojunction (BHJ). Figure 8 shows the device geometries and schematic band diagrams of these three OPV devices. [41] This evolution was to develop an optimal device geometry that can strategically address both short exciton lifetime issues and facilitate efficient charge extraction and transport.

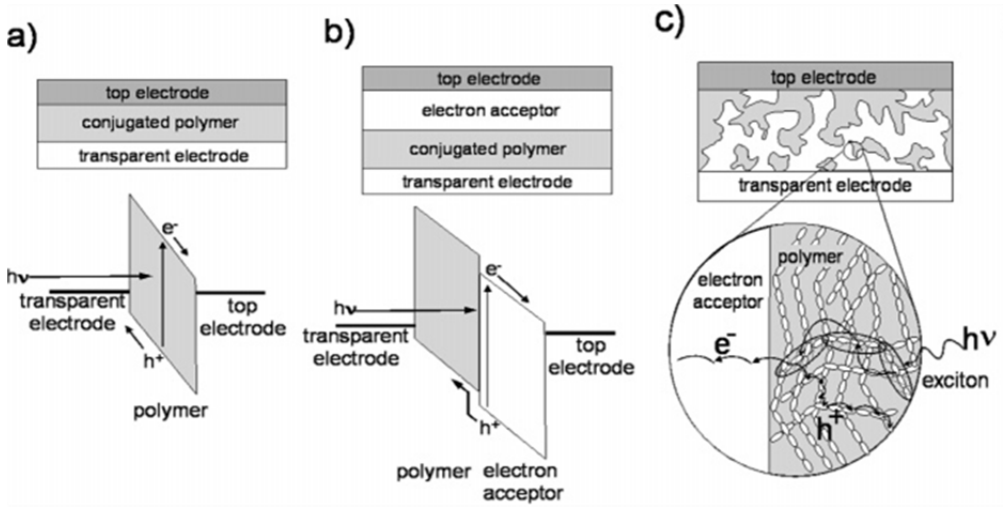

Figure 8. Device geometry and schematic band diagram of three different OPV devices: a) single layer, b) PHJ and c) BHJ OPVs. Reprinted with permission from Chem. Mater. 16, 4533 (2004). Copyright 2004 American Chemical Society.

During the nascent stage of OPV development, single layer OPV cells were developed. A single layer OPV is the simplest form of OPVs in terms of device geometry, where an organic single layer is positioned between two asymmetric contacts. The first OPV was reported by Kalmann *et al*. [42] in 1958. They fabricated an OPV cell by using a single layer of anthracene crystal sandwiched by two NaCl solutions contacted by silver electrodes. In 1982, Weinberger *et al*. [43] reported a polyacetylene based single layer PSC. Efficiencies of these single layer OPV devices were far less than 1 %, due to the intrinsic drawback of exciton lifetime. In single layer OPVs, charge dissociation occurs at the organic-electrode interface. However, excitons rarely reach the organic-electrode interface as they decay before reaching the interface due to their short lifetime and even though they reach the interface and dissociate into charge carriers, most of the electrons will recombine with holes rather than collected by electrodes. Hence, their photocurrent is significantly limited by the exciton diffusion length.

Tang proposed a bilayer, or planar heterojunction (PHJ) device geometry in 1986 in an attempt to solve this issue [44]. In the PHJ OPV devices, a second organic semiconductor layer is incorporated between the first organic layer and the cathode. The second organic layer has a lower LUMO level than the first organic layer and thereby electron accepting. The key feature of a PHJ structure is that the charge dissociation occurs at the donor-acceptor interface, as opposed to the organic-electrode interface. The large energy difference, leading to the strong electron withdrawing potential, must exceed the exciton binding energy. If an exciton reaches the donor-acceptor interface, an electron can transfer to the acceptor semiconductor and a hole can transfer to the donor

semiconductor. Subsequently, electron and hole travel in the opposite direction to be collected by the electrodes. Tang reported a PCE about 1 % under simulated Air Mass 2 (AM2) illumination in his PHJ OPV comprised of copper phthalocyanine (CuPc) and perylene tetracarboxylic derivative [44] and this record stood for a decade.

Even though the PHJ device geometry allows for less lossy mechanism than single layer device geometry in terms of charge transport and collection, exciton lifetime issues still remained. Only excitons generated within their diffusion length to the donor-acceptor interface can contribute to the photocurrent generation. Therefore, the exciton lifetime issue should be addressed by narrowing the distance between the bulk donor region where excitons are generated by light absorption and donor-acceptor interface where excitons are dissociated. However, reducing the thickness of the active layer cannot be a solution as it is detrimental to absorption of light.

Major advances in term of device geometry were made in 1995 by two groups. Yu *et al*. [45] and Halls *et al*. [46] introduced the idea of bulk heterojunction (BHJ) geometry. In BHJ OPV devices, donor and acceptor organic materials are interspersed with each other to extend their interface area throughout the active layer. BHJ effectively reduces the distance between the donor and the donor-acceptor interface, thereby allowing for higher probability of generation of excitons close to the interface and their dissociations into free charge carriers. Ideally the length scale of the blend is close to the exciton diffusion length, and hence every photon absorbed in the active layer can potentially contribute to the photocurrent. To fabricate a BHJ, the interpenetrating network of donor and acceptor with a bi-continuous phase separation is formed by

dissolving both polymers in the same solvent, followed by casting into a single blended layer. Phase separation can occur while the solvent evaporates and during post-deposition annealing. It is serendipity that the phase separation nanomorphology length scale that Mother Nature provides between the donor and acceptor materials is commensurate to the OPV exciton diffusion length. For small-molecule OPVs, both donor and acceptor molecules are co-evaporated in vacuum. Since its inception, BHJ has been the mainstream of OPV research in terms of device geometry so far.

Figure 9 shows an ideal OPV device geometry [47]. This design also allows for a significantly longer optical path length, orthogonal to the charge motion, thus decoupling the optical and electrical constraints. The donor and acceptor phases are interspaced by around the exciton diffusion length so that excitons efficiently reach the D-A interface by diffusion. In addition, charge carriers can transport to the electrodes via the interdigitated and percolated "highways" [47]. This geometry enables efficient charge separation, however, is not easy to obtain in classical polymer mixture due to the disordered nature of polymers [47], and the control of the interface quality.

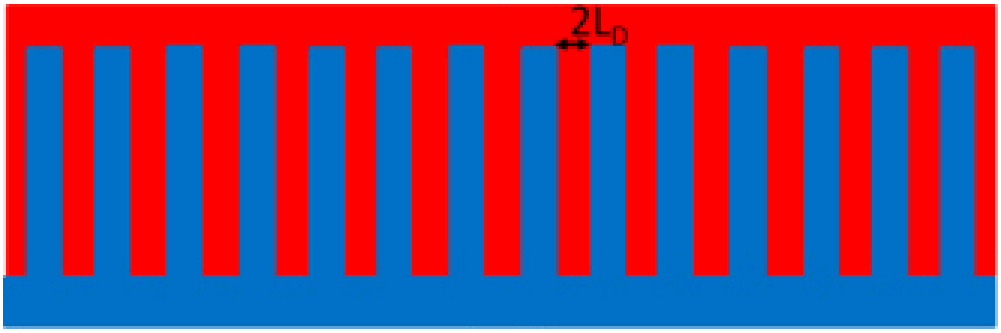

Figure 9 Ideal OPV device geometry. Reprinted by the creative commons attribution license from Prog. Polymer. Sci. 38 1929 (2013).

2.3.2. Material selection

Subsequent to the discovery of conducting polymers, a variety of conjugated polymers, in terms of solubility, stability, and electrical conductivity, have been synthesized in the 1990s. Consequently, various combinations of donor and acceptor materials have been used for PSCs to enhance their PCEs. The most widely used combination for BHJ PSCs is a blend of a semiconducting polymer as a donor and buckminsterfullerene (C60) derivative. Buckminsterfullerene (C60) has been the dominant acceptor used ubiquitously in both small molecule OPVs and PSCs, owing to its deep LUMO level and high electron mobility. Furthermore, pioneering discoveries in 1992-1993 demonstrated its ideal charge separation kinetics in combination with donor polymers, by providing sufficient energetics for exciton dissociation. Sariciftci *et al* [48] reported ultrafast photoinduced electron transfer from MEH-PPV onto fullerenes at the interface upon illumination by observing photoluminescence quenching in a thin layer PHJ of MEH-PPV and C60. Subsequently, Lee *et al*. [49] reported that the steady-state photoconductivity of conjugated polymers increased by several orders of magnitude upon adding C60. PCBM, a soluble derivative of buckminsterfullerene, remains the most popular electron transporter in PSCs.

For donor polymers, poly(phenylene vinylene) (PPV) was widely used from the mid 1990s till the early 2000s. The two representative PPV-based materials are poly[2-methoxy-5-(2-ethylhexyloxy)-1,4-phenylenevinylene (MEH-PPV) and poly(2-methoxy-5-(3′,7′-dimethyloctyloxy)-1,4-phenylene vinylene (MDMO-PPV) and they exhibited

similar photovoltaic properties. Numerous studies focused on PPV:PCBM BHJ PSCs not only for achieving higher efficiencies in PSCs, but also for better understanding of phase separation [50-51], carrier mobilities [52], and the origin of the open-circuit voltage [37].

For a decade since it was first reported back in 2002 [39], P3HT had received tremendous interest as an attractive replacement to PPV-based materials for PSC research. P3HT has advantages over PPV-based materials in that it has reduced bandgap and high hole mobility exceeding 0.1 cm^2 / Volt·sec, with proper morphology control. The absorption edges of MEH-PPV and MDMO-PPV are around 550 nm, whereas the absorption edge of P3HT is around 650 nm, which matches the sun's maximum photon flux in the range between 650 and 700 nm. P3HT:PCBM has been the baseline model of single PSC research and remarkable improvement in reported PCEs has been achieved [38].

2.3.3. Nanomorphology control by process optimization

As described in the above, the morphology of the active layer in BHJ structure plays an important role in efficient charge dissociation and transport. Refined morphology effectively widens the interface area and provides a continuous percolation pathway, allowing for higher probability of exciton dissociation and charge transport, respectively. Propelled by the advances in the development of high resolution scanning probe microscopy techniques, including scanning electron microscopy (SEM), atomic force microscopy (AFM), and transmission electron microscopy (TEM), extensive

investigation on morphology of active layers within PSCs has been reported and contributed to enhancing PCEs.

Shaheen *et al.* [53] reported 2.5 % efficiency in MDMO-PPV:PCBM PSCs. They investigated the effect of two different solvents: toluene and chlorobenzene (CB). The device with a CB-cast active layer showed enhanced Jsc and threefold PCE increase compared to that with toluene-cast active layer. Authors analyzed PCBM domains in surface morphology of these two devices. The PCBM domains in CB-cast active layer were smaller than those in toluene-cast active layer, thereby yielding increased charge carrier mobility and facilitated enhanced electron collection. This was further supported by TEM and cross-sectional SEM image that show better mixing of PCBM domains with the blend. [53]

Van Duren *et al*. [54] presented a comprehensive study on optimal ratio of MDMO-PPV:PCBM PSCs. Among devices with varying ratio of MDMO-PPV and PCBM dissolved in CB, maximum efficiency was achieved in 1:4 composition of MDMO-PPV:PCBM. Authors related higher PCBM of the optimal ratio to charge mobility and phase separation. With higher PCBM, both electron and hole mobility increase. Moreover, phase separation occurs only at higher PCBM, reducing carrier recombination. [54]

Research on P3HT:PCBM was spurred by the superior properties and optimal combination of P3HT and PCBM [38]. Moreover, having benefited from the understanding of the fundamental device physics with insight into process optimization

gained from the research on PPV:PCBM [55], the efficiency of P3HT:PCBM PSCs has significantly improved.

It is difficult to conclude the exact one-size-fits-all ratio that works best for all P3HT:PCBM PSCs, because endogenous properties, such as regio-regularity, polydispersity and molecular weight are different in all polymers used in experiments, depending on the suppliers and batch. Furthermore, PCEs also depend on the thickness of the active layers. During the early stage of P3HT:PCBM research, Schilinsky *et al*. [39] and Padinger *et al*. [56] studied compositions between 1:2 and 1:3 ratio of P3HT:PCBM and reported 2.8 and 3.5 percent PCEs, respectively. However, according to subsequent studies on composition of P3HT:PCBM PSCS, consensus has been made that the optimal ratio of P3HT and PCBM is 1:1~0.8. Chirvase *et al*. [57] showed the maximum PCE occurs between 1:1 and 1:0.9. Huang *et al*. [58] used time-of-flight technique to show balanced mobility of both electron and hole at the composition of 1:1 weight ratio, which is attributed to the formation of a more-ordered structure in the blend. Li *et al*. [59] and Reyes-Reyes *et al*. [60] reported 4.4 % and 4.9 % PCEs, respectively, at an optimal ratio of 1:0.8.

Thermal annealing has been known to enhance overall PCEs of P3HT:PCBM PSCs. The main reason behind this enhancement is that annealing improves morphology of P3HT:PCBM film. To elaborate, enhanced crystallinity of P3HT and improved charge carrier mobility upon annealing [61] lead to improved PCEs. Annealing temperature should be between the glass transition temperature and the melting point of the polymers, which is 12 °C and 178 °C for P3HT [62]. Numerous studies were reported regarding

effect of annealing on morphology of P3HT:PCBM film and most of them were performed with thermal annealing at temperatures from 110 °C to 160 °C for 1-30 minutes. [38] Chirvase *et al*. [57] studied optimum annealing duration on P3HT:PCBM devices annealed at 130 °C. They observed a red shift in P3HT absorption. The red shift was more dramatic in devices with longer annealing duration. Moreover, the absorption shoulder around 620 nm was also pronounced in devices with longer annealing duration, indicating interchain interaction of P3HT, and a higher degree of interchain ordering. Reyes-Reyes *et al*. [60] analyzed the performance characteristics of devices annealed at different temperatures and durations. They obtained the maximum J_{SC} of 11.1 mA/cm^2 in the device annealed at 150 °C for 5 minutes, owing to improved film crystallinity. Li *et al*. [59] demonstrated better improvement in PCE in devices annealed after cathode deposition in comparison to those annealed before cathode deposition. Authors speculated the cathode acts as a barrier that hinders morphology improvement. They also reported that high roughness and coarse texture shown in AFM image of optimally annealed film (110 ° C, 10 minutes) lead to better contact between polymer and cathode, and thereby facilitate charge collection. Erb *et al*. [61] reported a more systematic study on the correlation between crystallinity of P3HT:PCBM and their optical properties. They provided a clearer explanation on the effect of annealing; upon annealing isolated PCBM molecules begin to diffuse into larger aggregates, and P3HT aggregates can be converted into P3HT crystallites in these PCBM-free regions, as shown in Figure 10. They concluded that enhanced PCE in annealed P3HT:PCBM devices is attributed to better electron transport in the PCBM clusters and enhanced absorption of P3HT crystallites.

Subsequently, Ma *et al*. [63] achieved a 5 % PCE in P3HT:PCBM PSC annealed at 150 ° C for 30 minutes.

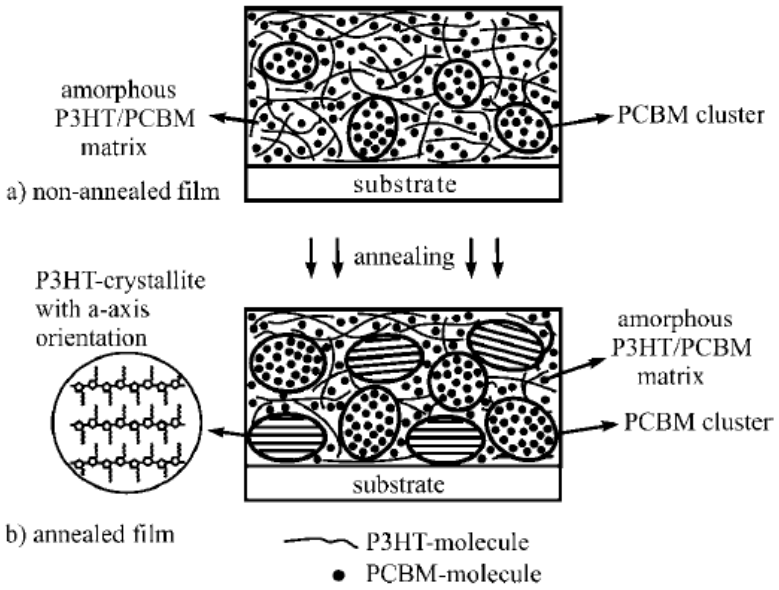

Figure 10. Schematic change of P3HT:PCBM films upon annealing. Reprinted with permission from Adv. Func. Mater. 15, 1193 (2005). Copyright 2005 WILEY-VCH Verlag GmbH & Co. KGaA, Weinheim.

Thermal annealing is a simple method of improving efficiency of PSC, but room-temperature annealing is more feasible for large-area, flexible PSCs. [64-68] Room-temperature annealing, or "solvent-annealing" is a method to control the growth rate of active layer, by exposing the solution-processed active layer to solvent vapor. Li *et al*. [64] achieved 4.4 % PCE in a P3HT:PCBM cell by using solvent annealing method. 1,2-Dichlorobenzene (oDCB) was used as a solvent for spin casting of polymers to decelerate solvent evaporation because of its higher boiling point. Authors compared PSCs with different growth rates by varying the solvent evaporation time and showed that slow-grown films show better performance than fast-grown films. By analyzing charge carrier

mobility and absorption data, authors concluded that the PCE improvement is attributed to a high-degree of ordering of the polymer by self-organization. Effectiveness of solvent annealing was supported by Mihailetchi *et al*. [65], who showed that the hole mobility was improved by 33 times in slow-grown films. Overall, in the body of published literature, the aggregate average PCE efficiency for P3HT:PCBM based OPVs is around 3.5% [38]. Figure 11 shows the standard configuration of P3HT:PCBM baseline model.

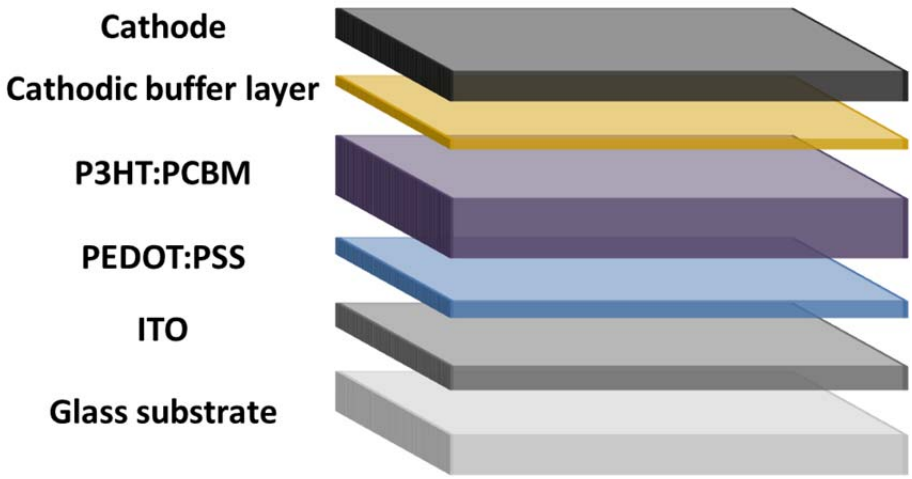

Figure 11. Standard configuration of P3HT:PCBM baseline model.

2.4 Cost and Lifetime of Organic Photovoltaics

For the last three decades, OPV research has mainly focused on achieving higher efficiencies. Through sophisticated device geometry, tailored development of new polymers benefited from their synthetic flexibility, and heuristic morphology control aided by various nanoscale microscopy technologies, NREL-certified efficiencies of

PSCs reached 10.6 [69] and 11.5 [70] percent in tandem and single cells, respectively. Figure 12 shows the NREL-certified research cell record efficiency chart.

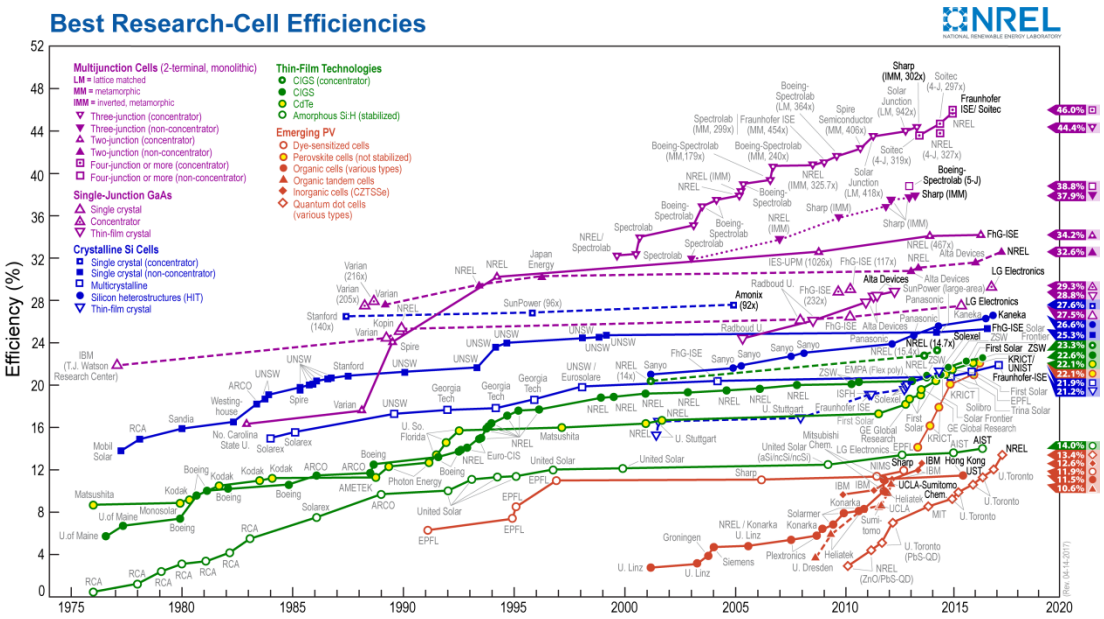

Figure 12. Research cell record efficiency chart published by NREL.

Even though remarkable improvement has been made in three decades, current PCE of PSCs is not comparable to that of the highest inorganic counterparts, e.g. ~ 44 percent, for triple junction solar cells. However, unique properties of OPVs, such as large area scalability, synthetic flexibility of organic materials as well as mechanical flexibility of OPV cells, and lightness may find potential niche market opportunities, particularly for point-of-use applications, such as wearables. For instance, they may be especially useful for domestic applications, such as powering autonomous Internet-of-Things objects, because they are known to perform well under diffuse light [71] and they

are spectrally matched better to indoor lighting, which is predominately in the visible range, with less infrared components.

In addition to efficiency, cost is another indispensable parameter that governs technical and commercial viability of PV technologies. Importance of cost is underlined in applications that do not require high efficiency PV cells. Low-cost processing capability has always been the main thrust and excitement for OPV research, but there are other costs that contribute to cost-of-ownership of completed OPV modules. An OPV cost analysis reported in 2011 [72] revealed that cost of raw materials occupies the lion's share in the production of OPV module, up to 80 %. As shown in Figure 14, most of the material cost is attributed to ITO coated on PET (maximum 51.2 percent of the total material cost), and P3HT:PCBM active layer (maximum 27.2 percent of the total material cost). [72] P3HT and PCBM are specialty chemicals, but PCBM is more than 12 times more expensive than P3HT. However, PET, ITO and PCBM are respectively, the predominant flexible substrate, anode and acceptor materials for PSCs and their candidate replacements have yet to demonstrate both superior performance and cost effectiveness over them. Consequently, there is not much room for improvement in cost of OPVs.

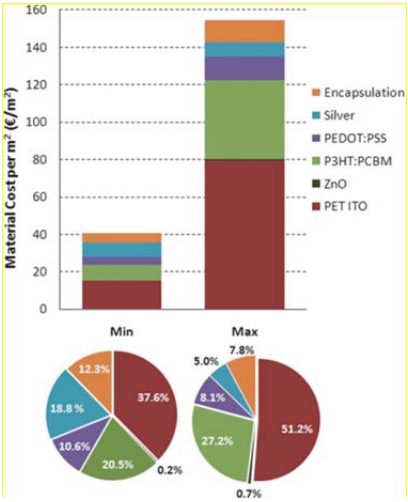

Figure 13. Absolute (top) and fractional (bottom) costs of materials used in the manufacture of a $1m^2$ OPV module. Reprinted with permission from Energy Environ. Sci., 4, 3741 (2011). Copyright 2011 The Royal Society of Chemistry.

Coupled with efficiency and cost, lifetime also plays a penultimate role in potential commercialization of PV technologies. These three parameters are interdependent and relative importance of each parameter depends on applications. Importance of lifetime is underlined in OPVs because they are known to degrade in ambient air, mostly because of moisture and oxygen. Furthermore, ironically, UV light and high temperature are also known as sources of OPV degradation. [73] These sources of degradation, and their combination affect each layer and their interfaces in OPVs. Therefore, OPV cells are generally fabricated inside the glove box filled with inert gas, i.e. nitrogen or argon. In addition to these technical issues, an economic analysis on OPV devices revealed that elongated lifetime significantly reduces levelized energy cost (cent/Kwh) [74].

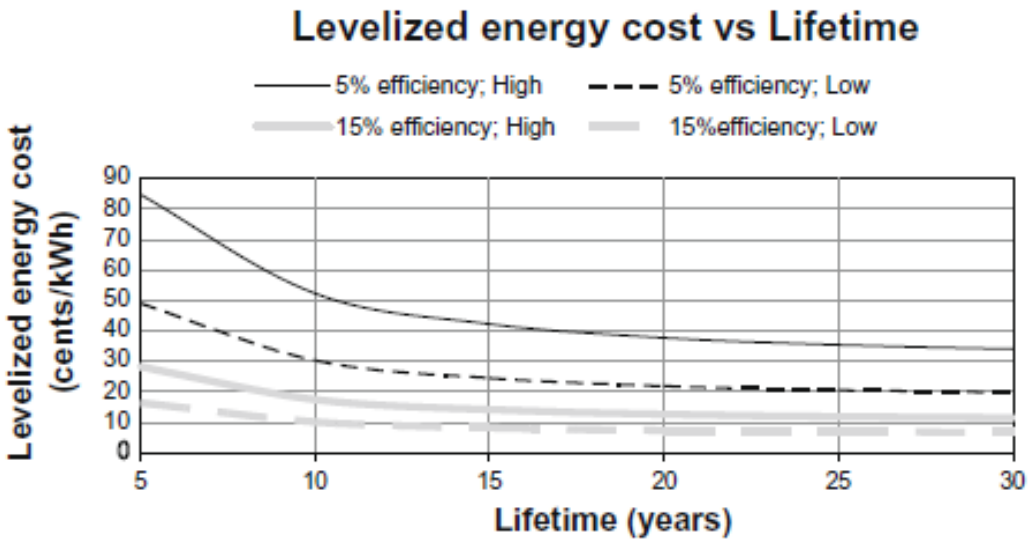

Figure 14. Levelized energy cost (cents/kWh) versus lifetime (years). Reprinted with permission from Sol. Energy, 83, 1224 (2009). Copyright 2011 Elsevier Ltd.

As shown in the levelized energy cost versus lifetime graph in Figure 14, the cost reduction effect is maximized when the efficiency of OPV device is low. In this sense, increased lifetime of OPV by hermetic encapsulation and hermetic sealing strategies enhances technical feasibility and economic viability by reducing operational cost as well as compensating efficiency for niche market opportunities [74].

To address these technical and economic issues, OPV cells are often encapsulated before exposure to ambient air. The most preponderant encapsulation method is by using two barrier films and a sealant; OPV cells are sandwiched between front and back barrier films, whose edges are glued together by the sealant. Therefore, OPV cells can be protected vertically by barrier films and horizontally by the sealant.

Chapter 3

Hermetic Encapsulation of Organic Photovoltaics

Various sources of the degradation from ambient air were identified: moisture, oxygen, light, temperature, and their combination, and in some instances the chemical moieties and reaction byproducts of experimental and commercially available sealants and encapsulants. Among them, moisture and oxygen are known to be the most common and pernicious, as they lead to chemical degradation of active layer, the reactive cathode (i.e. Ca) and even the interface between them [73], as well as experiencing thermal and UV enhanced oxidative and hydrolytic degradation mechanisms.

For longer operational lifetimes, various encapsulation schemes were suggested. These include sophisticated encapsulation schemes, such as a sealed glass container or a high vacuum chamber [75-76]. Edge-sealed and laminated approaches are less complex and more preponderant. In both schemes, an OPV cell is sandwiched between impermeable front- and back-sheets, which prevent moisture or oxygen ingress over the face area of the cell. Edge sealant or laminating adhesive is used to protect the OPV cell from edge ingress of permeants.

3.1 Requirements of Encapsulation Materials for Organic Photovoltaic Applications

Both barrier films and sealants are required to have thermal and light stability for outdoor applications, not to mention ultra-low gas permeability. The water vapor transmission rate of 10^{-6} $g \cdot m^{-2} \cdot day^{-1}$ and oxygen transmission rate of 10^{-3} $cm^3 \cdot m^{-2} \cdot day^{-1}$ are often used as a criteria for gas permeability [77]. In addition, flexibility is another requirement for both barrier films and sealants so that they are amenable to roll-to-roll processing, thereby OPV cells can retain their cost effectiveness. Moreover, very high transmittance is desirable for front barrier films as they optically couple with OPV cells. Last but not least, thermally curable encapsulants are required to be cured at a temperature lower than the glass transition temperature of flexible substrates and the annealing temperature of bulk heterojunction OPV devices, typically lower than 150 ºC.

The aforementioned triumvirs, i.e. efficiency, cost, and lifetime are interdependent and need to be balanced so that lifetime enhancement by encapsulation does not seriously sacrifice efficiency nor cost effectiveness. In other words, encapsulation processing is required to be compatible with low-cost and low-temperature processing to fully take advantages of OPV devices and to avoid thermally induced degradation of OPV performance, respectively.

Moreover, encapsulants are required to have the same driving forces of OPV devices, such as lightness and flexibility to be amenable to their unique applications, for instance, window tinting applications, building integrated photovoltaic applications, and

portable or wearable energy source. The inorganic edge-sealing technology has proven its long term hermetic sealing capability and is an attractive approach for flat, rigid substrates [78]. However, it is not suitable for flexible OPVs. Currently used organic edge-sealants can be flexible, but their relatively higher gas permeability has been of concern [78]. As an alternative to inorganic sealants and organic sealants, a combination of organic and inorganic materials was used to take advantage of flexibility of organic materials, while retaining low gas permeability in multilayered architecture [79]. Various groups used single layer, thermally-curable, polymer composite and multilayered films for OPV encapsulation and demonstrated improved lifetime compared to unprotected OPV cells [79]. By incorporating inorganic materials into the polymer, their gas permeability can be substantially improved, while maintaining flexibility.

Additionally, transparency is another requirement for encapsulants as they optically couple with OPV devices. Chemical inertness with the underlying layer of OPV devices is also an indispensable factor for encapsulants. However, those features are not critical requirements for edge-sealants as long as they do not cover the surface area of OPV devices. Last but not least, thermal and ultraviolet (UV) stability are required so that encapsulants and sealants do not degrade over time in an outdoor environment.

Ethylene vinyl acetate (EVA) was developed in an effort to forage for an economical substitute of silicone-based hybrid sealant and encapsulant, e.g. polydimethylsiloxane (PDMS), which has been the dominant PV encapsulant. However, consensus has been made that even though EVA has cost advantages and reasonable gas permeability, proven from food packaging industry, it does not have the best combination

of optimal properties; the presence of hydrolytically unstable ester bonds in the backbone of EVA and other commercial organic sealants such as polyvinyl butyral (PVB) leads to reduction in viscosity facilitated by depolymerisation, allowing creep and/or delamination to occur more easily [80]. Furthermore, the bond dissociation energy of carbon-carbon bonds in the backbone of EVA is 83 kcal/mol, corresponding to photons with wavelength of 343 nm. In contrast, the bond dissociation energy of Si-O bonds in the backbone of PDMS is ~108 kcal/mol, corresponding to photons with wavelength of 263 nm. No presence of terrestrial solar irradiation at 263 nm, compared to ordinary presence of solar irradiation at 343 nm, exemplifies the reasons for the exceptional UV stability of PDMS [80], which is also supported by experimental results under accelerated UV light environment. [81]

Though PDMS has been commonly used as a sealant, its high optical transmission and chemical inertness, coupled with UV stability are seemingly more suitable for encapsulants. Relatively higher moisture permeability and cost are still of concern, but can possibly be tolerated if used in combination with sealants with higher gas permeability that can mitigate its cost by longer lifetime. Furthermore, some recent studies demonstrated that the generally conjectured value of 10^{-6} $g \cdot m^{-2} \cdot day^{-1}$ for water vapor transmission rate (WVTR) derived from organic light emitting diode technology should not be considered as a golden rule and medium barrier materials with a WVTR around 10^{-3} $g \cdot m^{-2} \cdot day^{-1}$ can effectively protect OPV cells. [33, 82-83] Use of less moisture-sensitive active layer materials such as poly[9'-hepta-decanyl-2,7-carbazole-alt-5,5-(4',7'-di-2-thienyl-2',1',3'-benzothiadiazole) (PCDTBT) [84], more stable device

architecture and/or electrode materials can alleviate high moisture permeability requirements. For instance, inverted OPV structure was suggested as a more stable device architecture than conventional structures by enabling the removal of low work function electrodes [85-87]. Figure 15 shows the conventional and inverted PSC structures.

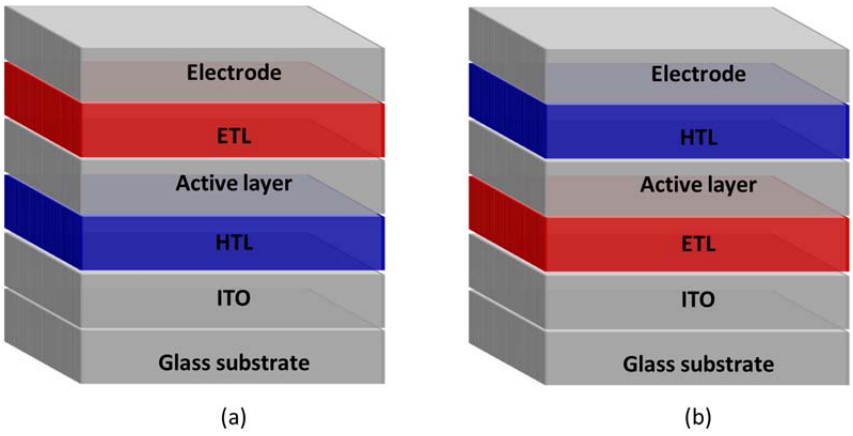

Figure 15. (a) Conventional and (b) inverted structure of PSC

More recently, Zhou *et al*. proposed polymer surface modifier as an alternative to reactive electrodes and demonstrated all polymer solar cells [88]. It can be inferred that the PDMS family of polymer based compounds should not be excluded from viable candidate sealants and encapsulants for certain OPV designs and applications. Hence, sealant materials for OPV should be selected based on the intended specific application; requirements such as barrier specifications, light stability, and flexibility requirements vary in different applications. The sealant, encapsulant and/or the dual sealant-encapsulant needs to be engineered and formulated for the specific device and end-use application.

3.2 Development of Organic-Inorganic Hybrid Sealants

We developed multi-component hybrid sealants, formulated with high solids, thermally curable binder resins that may be utilized as both encapsulants and edge-sealants in certain applications. Oxygen interactive components were blended with the resin so that they can self-organize to the outside of the seal. Inorganic nanoparticles were used to enhance the sealing properties and to provide the desired rheology control. The formulations are compatible with low-cost, low-temperature processing of OPV; they are screen-printable and curable at 130 ºC in 15 minutes. In addition, they have excellent flexibility and chemical resistance as well as good adhesion to glass and polyimide substrates. The detailed synthesis route and formulation processes are proprietary.

3.3 Preparation of Test Specimens

Polyimide films were used as a convenient flexible substrate that withstands higher temperatures, because its semi-transparency and amber color make it easier to visualize the oxidation of Calcium. Polyimide Kapton® Type HN films, just 25 micrometer thick, were cut into square pieces with side dimension of 25 mm and cleaned with isopropyl alcohol, followed by nitrogen blow-dry. Specimens were placed on a hot-plate to completely remove remaining moisture on the surface prior to metal evaporation.

Specimens were loaded into the thermal evaporator inside the glovebox for Ca deposition and pumped down overnight. The base pressure was ~10^{-7} Torr. 200 nm of Calcium was deposited atop the specimens under a pressure in the range of 10^{-6} Torr. Thickness and deposition rate were monitored by an acoustic crystal thickness monitor. The deposition rate was carefully controlled by first maintaining slow deposition rates (1-2 Å/sec) to promote good adhesion and then raising the deposition rate (5 Å/sec) after depositing 20 nm to produce a thick high-purity Ca layer.

Two 1.6-mm-thick square glass plates with side dimension of 76.2 mm were scrubbed and rinsed with isopropyl alcohol. 1 mL of two different hybrid sealants was applied using brush throughout the perimeter, centered at 12.5 mm from the edge of the bottom glass plate. The width of the sealant was 15 mm. This bottom glass plate was placed on a digitally-controlled hot plate, preheated to 130 ºC inside a glove box. After 2 minutes, calcium specimens were placed at the center of the glass plate and heated for 1 minute. A piece of identical cover glass was aligned onto the bottom glass to sandwich the Ca test specimens and four 25 g weights were placed on each perimeter of glasses to facilitate adhesion by adding pressure. Weights were preheated so that heat is not dissipated through them. This composite sealing structure was heated for 12 minutes for curing and taken out from the glove box after cooling down.

The control sample was prepared by using PDMS sealants to compare the sealing capability of our sealants with the existing commercial hybrid sealant. Dow corning Sylgard® 184 silicone elastomer base and curing agent were thoroughly mixed with ratio of 10:1 and applied on the bottom glass plates in the same ways as our hybrid sealant

samples. The control samples were cured at 140 ºC, for 30 minutes. All the samples showed good adhesion to glass plates.

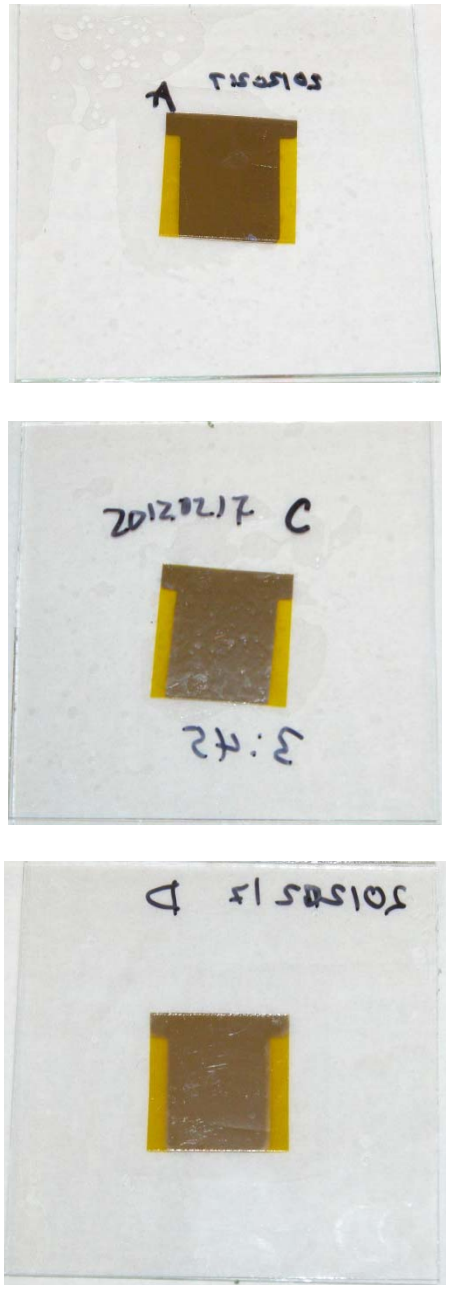

Figure 16. Composite sealing structure after lamination using prototype sealant A (top), prototype sealant C (middle), and PDMS control sample (bottom). The T-shaped calcium layer (metallic shiny, but appeared as dark grey in the photos here) deposited on top of the polyimide film is shown.

Figure 16 shows the composite structure after sealing with prototype sealant A, prototype sealant C, and PDMS control sample. Calcium specimens, where 200 nm calcium is deposited on top of the polyimide film, are located at the center of the composite structures. The T-shaped calcium layer was translucent metallic shiny (but appears dark grey in Figure 16) and the amber-colored "wings" are the part of polyimide film where calcium is not deposited.

3.4 Sealant Test Method

Calcium corrosion test has been widely used to determine the moisture and oxygen ingress to the specimens. The change from a mirror-like translucent shiny metallic film to a transparent calcium hydroxide film allows for easy determination of oxidation. Various methods to quantify the Calcium corrosion, i.e. WVTR were proposed, including optically, electrically, and volumetrically [89-92]. Volumetric measurements require complicated measurement systems. Optical and electrical methods are mostly developed to assess the performance of encapsulation barrier films. However, moisture and oxygen ingress through sealant is different from that through encapsulation barrier films in that the former is horizontal whereas the latter is vertical. For this reason, modification of those characterization methods and/or development of new characterization are required to quantify the horizontal moisture ingress through sealant. Measurement of the distance of moisture penetration from the edge to the center was used

to assess the performance of edge-sealants. However, it is agreed that calcium corrosion test is mostly useful for qualitative preliminary test purpose [92].

There has been long and urgent need for standards of accelerated weathering test for OPV cells. As sealants with improved sealing capability are being developed, 85 ºC / 85 % condition has been commonly used to shorten the time required to observe degradation. However, it was pointed out that the test result under this condition does not provide sufficient information to predict actual lifetime under normal operating condition due to the large variance and reliability in reported scaling factor between normal operating condition of OPV cells, typically between 25 ºC and 50ºC, and 85 ºC.

Chapter 4

Demonstration of Hybrid Sealants by Calcium Corrosion Testing

4.1 Calcium Corrosion Test Result

Samples were taken out from the glovebox and placed in ambient air, where temperature ranges from 18ºC to 25ºC and humidity ranges from 55% to 79%. Ca corrosion was observed to monitor the penetration of moisture. Horizontal permeation of moisture via edge-sealants leads to corrosion of the calcium layer, which can be observed by the color change in calcium specimens: the translucent metallic shiny calcium layer to the transparent calcium hydroxide. Since calcium layer was deposited on top of the polyimide film and calcium hydroxide is transparent, calcium corrosion will "expose" the amber color of the underlying polyimide film.

Multiple chemical reactions of calcium with oxygen and water were identified, all of which are thermodynamically favorable. However, higher solubility of water in polymers, compared to that of oxygen results in about 100~10000 times higher permeabilities for water than oxygen [89]. Furthermore, it has been shown that at room temperature, corrosion directly from water is significantly slower than via water [89].

Therefore, it was inferred that the following reaction of calcium with water is the most dominant mechanism.

$$Ca + 2H_2O \rightarrow Ca(OH)_2 + H_2$$

Figure 17. Composite sealing structure after 1960 hours exposure to ambient air, left: PDMS control sample and right: prototype sealant C. Note that calcium was completely corroded in the structure sealed with PDMS control sample in 22 to 24 hours, as evidenced by complete "exposure" of the amber-colored polyimide film underneath the transparent calcium hydroxide. The T-shaped calcium layer (metallic shiny, but appears white in this photo) is shown on the right.

Figure 17 shows the composite structures after exposure to ambient air for 1960 hours. In the PDMS sample, shown on the left, calcium was completely corroded in 22 to 24 hours, as evidenced by the complete "exposure" of the amber-colored polyimide film underneath the transparent calcium hydroxide. In the meanwhile, in the sealant C sample, most of the T-shaped calcium layer (metallic shiny, but appears white in this photo) remained, implying that calcium corrosion is by far less significant, even after 1960 hours

exposure to ambient air. Evidence of slight calcium corrosion is shown in Figure 17, by the reduced size of the T-shaped calcium layer, as compared to that in Figure 16. The transparent calcium hydroxide layer "exposed" the underlying polyimide film, so the remaining calcium layer in Figure 17 appears smaller than that in Figure 16. Multiple pathways lead to calcium corrosion in the edge-sealed structure and they can be classified as endogenous factors and exogenous factors. The former includes byproducts evolved during curing process and reacting with calcium. Intrinsic defects of sealing structure are in the same category and facilitate reaction of calcium with water. In contrast, the latter includes edge ingress of permeants either through sealant or between glass and edge-sealant. Delamination or bubble formation provides a weak link for calcium corrosion by allowing for edge ingress of permeants between glass and edge-sealant [92]. Delamination results in direct permeation path from ambient air to calcium, whereas bubble formation effectively shortens the permeation path length, facilitating calcium corrosion. It is notable that bubble formation in the PDMS sample was not as notable as in the sealant C, implying superior gas permeability of the sealant C, compared to PDMS. Moreover, homogeneous and diffuse oxidation edge in the sealant C sample implies that endogenous factors can be eliminated from the source of calcium corrosion. In addition, it is inferred that bubble formation, leading to edge permeation between glass and edge-sealant, did not critically affect calcium corrosion. This implies that reduced effective permeation length is still sufficient to prevent moisture ingress owing to good gas permeability of the sealant C or the nitrogen gas was trapped during curing process and formed bubbles, effectively protecting calcium. However, the source of bubble is still

unknown; it can be trapped nitrogen gas, byproduct gas generated and trapped during curing process, and localized delamination due to insufficient pressure or flow of sealant. We agreed that further optimization of curing process and nanoparticle inclusion is required to apply uniform pressure and/or control rheology, so that localized failure of edge-seal can be minimized.

Figure 18 shows the composite structures of the sealants A and C after exposure to ambient air for 1960 hours. The T-shaped calcium layer appears grey and white in the sample A and C, respectively in Figure 18. Calcium in sample A does not show any notable oxidation, except slightly blurred edge on the top left side. Presumably localized bubble formation and/or delamination on the top left side are responsible for the localized calcium corrosion. It is notable that except for edge-seal failure on top right side, bubble formation in the sealant A sample is much less than for sealant C. Both of our sealants show much better sealing capability than PDMS.

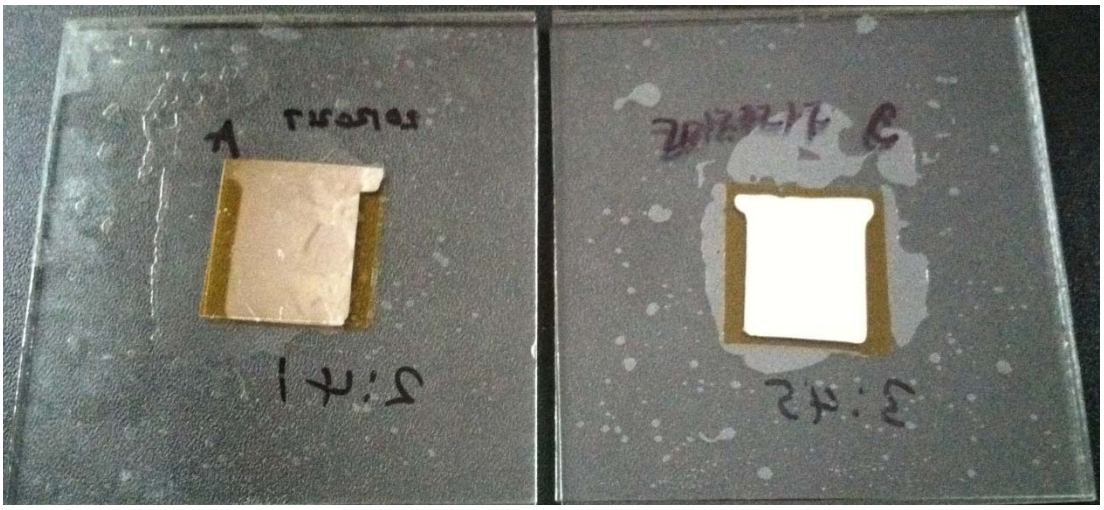

Figure 18. Composite sealing structure after 1960 hours exposure to ambient air, left: prototype sealant A and right: prototype sealant C. The T-shaped calcium layer (metallic shiny) appears grey on the left and white on the right in this photo.

4.2. Conclusion and Future Work

Decreased gas permeability by incorporating inorganic materials, coupled with flexibility of organic sealants, suggests technical feasibility of hybrid sealants. Our hybrid sealants have proven superior gas permeability compared to PDMS. However, their C-C bond is still susceptible to degradation by UV. Incorporating UV absorber will increase resistance to UV degradation, but adds material cost. It was shown that significant drop in transmittance was observed in organic sealants exposed to accelerated UV condition. However, unlike encapsulants, sealants do not serve the function of optical coupling with OPV devices, Thus, susceptibility to UV degradation does not necessarily exclude organic sealants and our hybrid sealants from technically viable candidates for OPV

encapsulation. Further optimization of our sealants for seal and rheology control, as well as curing process for good adhesion and minimization of bubble formation is underway.

Bibliography

[1] F. C. Krebs, “Fabrication and processing of polymer solar cells: a review of printing and coating techniques,” Sol. Energy Mater. Sol. cells 93, 394-412 (2009).

[2] T. F. O’Connor, A. V. Zaretski, S. Savagatrup, A. D. Printz, C. D. Wilkes, M. I. Diaz, E. J. Sawyer, and D. J. Lipomi, “Wearable organic solar cells with high cyclic bending stability: Materials selection criteria,” Sol. Energy Mater. Sol. Cells 144, 438-444 (2016).

[3] C.-C. Chen, L. Dou, R. Zhu, C.-H. Chung, T.-B. Song, Y. B. Zheng, S. Hawks, G. Li, P. S. Weiss, and Y. Yang, “Visibly transparent polymer solar cells produced by solution processing,” ACS Nano 6(8), 7185-7190 (2012).

[4] H. Ernst, “The use of patent for technological forecasting: The diffusion of CNC-technology in the machine tool industry,” Small Business Econ. 9(4), 361-381 (1997).

[5] M. Y. Jamali, A. Aslani, B. F. Moghadam, M. Naaranoja, and M. D. Madvar,”Analysis of photovoltaic technology development based on technology life cycle approach,” J. Renew. Sustain. Energy 8, 035905 (2016).

[6] S. Lizin, J. Leroy, C. Delvenne, M. Dijk, E. D. Schepper, and S. Van Passel, “A patent landscape analysis for organic photovoltaic solar cells: Identifying the technology’s development phase,” Renewable Energy 57, 5-11 (2013).

[7] J. S. Liu, C.-H. Kuan, S.-C. Cha, W.-L. Chuang, G. J. Gau, J.-Y. Jeng, “Photovoltaic technology development: a perspective from patent growth analysis,” Sol. Energy Mater. Sol. Cells 95, 3130-3136 (2011).

[8] H. Hoppe and N. S. Sariciftci, “Polymer solar cells,” Adv. Polym. Sci. 214, 1-86 (2008).

[9] S. Mori, H. Oh-oka, H. Nakao, T. Gotanda, H. Jung, A. Iida, R. Hayase, N. Shida, M. Saito, K. Todori, T. Asakura, A. Matsui, M. Hosoya, "Organic photovoltaic module development with inverted device structure," MRS Proceedings, vol.1737 (2015).

[10] M. Hosoya, H. Oooka, H. Nakao, T. Gotanda, S. Mori, N. Shida, R. Hayase, Y. Nakano, M. Saito, "Organic thin film photovoltaic modules," Proceedings of the 93rd Annual Meeting of the Chemical Society of Japan, 21–37 (2013).

[11] R. F. Service, “Outlook brightens for plastic solar cells,” Science, 332(6027) 293 (2011).

[12] H-J. Lee, T. Arai, Y. Takeuchi, N. Koide, L. Ham, M. Shimizu, “Improvement of efficiency of polymer solar cells with soluble fullerene derivatives,” 4th World Conference on Photovoltaic Energy Conversion (WCEP-4), Hawaii (2006).

[13] M. A. Green, K. Emery, D. L. King, Y. Hishikawa, W. Warta, "Solar cell efficiency tables (version 28)," Prog. Photovol.:Res. Appl. 14(5), 455–461 (2006).

[14] M. A. Green, K. Emery, D. L. King, Y. Hishikawa, W. Warta, "Solar cell efficiency tables (version 31)," Prog. Photovol.:Res. Appl. 16(1), 61–67 (2008).

[15] M. A. Green, K. Emery, D. L. King, Y. Hishikawa, W. Warta, "Solar cell efficiency tables (version 35)," Prog. Photovol.:Res. Appl. 18(2), 144–150 (2010).

[16] M. A. Green, K. Emery, D. L. King, Y. Hishikawa, W. Warta, "Solar cell efficiency tables (version 37)," Prog. Photovol.:Res. Appl. 19(1), 84–92 (2011).

[17] M. A. Green, K. Emery, D. L. King, Y. Hishikawa, W. Warta, "Solar cell efficiency tables (version 41)," Prog. Photovol.:Res. Appl. 21(1), 1–11 (2013).

[18] M. A. Green, K. Emery, D. L. King, Y. Hishikawa, W. Warta, "Solar cell efficiency tables (version 43)," Prog. Photovol.:Res. Appl. 22(1), 1–9 (2014).

[19] M. A. Green, K. Emery, D. L. King, Y. Hishikawa, W. Warta, "Solar cell efficiency tables (version 45)," Prog. Photovol.:Res. Appl. 23(1), 1–9 (2015).

[20] M. A. Green, K. Emery, D. L. King, Y. Hishikawa, W. Warta, "Solar cell efficiency tables (version 48)," Prog. Photovol.:Res. Appl. 24(7), 905–913 (2016).

[21] F. C. Krebs, S. A. Gevorgyan and J. Alstrup, “A roll-to-roll process to flexible polymer solar cells: model studies, manufacture and operational stability studies,” Journal of Material Chemistry, vol.19, issue 30, pp.5442-5451, 2009.

[22] L. Blankenburg, K. Schultheis, H. Schache, S. Sensfuss and M. Schröner, “Reel-to-reel wet coating as an efficient up-scaling technique for the production of bulk-heterojunction polymer solar cells,” Solar Energy Materials and Solar Cells, vol.93, issue 4, pp.476-483, 2009.

[23] F. C. Krebs, “Fabrication and processing of polymer solar cells: A review of printing and coating techniques,” Solar Energy Materials and Solar Cells, vol.93, issue 4, pp.394-412, 2009.

[24] G. Yu, J. Gao, J. C. Hummelen, F. Wudl, and A. J. Heeger, “Polymer photovoltaic cells: enhanced efficiencies via a network of internal donor-acceptor heterojunctions,” Science, vol.270, pp.1789-1791, 1995.

[25] J. J. M. Halls, C. A. Walsh, N. C. Greenham, E. A. Marsegila, R. H. Friend, S. C. Moratti and A. B. Holmes, “Efficient photodiodes from interpenetrating polymer networks,” Nature, vol.376, pp.498-500, 1995.

[26] H.-Y. Chen, J. Hou, S. Zhang, Y. Liang, G. Yang, Y. Yang, L. Yu, Y. Wu, and G. Li, “Polymer solar cells with enhanced open-circuit voltage and efficiency,” Nature Photonics, vol.3, pp.649-653, 2009.

[27] J. Peet, J. Y. Kim, N. E. Coates, W. L. Ma, D. Moses, A. J. Heeger, and G. C. Bazan, “Efficiency enhancement in low-bandgap polymer solar cells by processing with alkane dithiols,” Nature Materials, vol.6, pp. 497-500, 2007.

[28] Y. Liang, Y. Wu, D. Feng, S.-T. Tsai, H.-J. Son, G. Li, and L. Yu, "Development of New Semiconducting Polymers for High Performance Solar Cells," Journal of American Chemical Society, vol. 131, pp. 56-57, 2008.

[29] G. Li, V. Shrotriya, J. Huang, Y. Yao, T. Moriarty, K. Emery and Y. Yang, “High-efficiency solution processable polymer photovoltaic cells by self-organization of polymer blends,” Nature Materials vol.4, pp.864-868, 2005.

[30] G. Li, R. Zhu, and Y. Yang, “Polymer solar cells,” Nature Photonics, vol. 6, pp. 153–161, 2012.

[31] N. Ginley, “National solar technology roadmap: organic PV,” management report, NREL/MP-520-41738, 2007.

[32] M. C. Scharber, D. Mühlbacher, M. Koppe, P. Denk, C. Waldauf, A. J. Heeger, and C. J. Brabec “Design rules for donors in bulk-heterojunction solar cells-towards 10 % energy-conversion efficiency,” Advanced Materials, vol.18, pp. 789-794, 2006.

[33] S. Cros, R. de Bettignies, S. Berson, S. Bailly, P. Maisse, N. Lemaitre, and S. Guillerez, “Definition of encapsulation barrier requirements: a method applied to organic solar cells,” Solar Energy Materials and Solar Cells, vol.95, pp.s65-69, 2009.

[34] H. Shirakawa, E. J. Louis, A. G. MacDiarmid, C. K. Chiang, and A. J. Heeger, “Synthesis of electrically conducting organic polymers: halogen derivatives of polyacetylene, (CH)x,” J. Chem. Soc., Chem. Commun. 16, 578-580 (1977).

[35] B. A. Gregg and M. C. Hanna, “Comparing organic to inorganic photovoltaic cells: Theory, experiment, and simulation,” J. Appl. Phys. 93, 3605-3614 (2003).

[36] O. V. Mikhnenko, P. W. M. Blom, and T.-Q. Nguyen, “Exciton diffusion in organic semiconductors,” Energy Environ. Sci. 8, 1867-1888 (2015).

[37] K. Vandewal, K. Tvingstedt, A. Gadisa, O. Inganas, and J. V. Manca, “On the origin of the open-circuit voltage of polymer-fullerene solar cells,” Nat. Mater. 8, 904-909 (2009).

[38] M. T. Dang, L. Hirsch, and G. Wantz, “P3HT:PCBM, best seller in polymer photovoltaic research,” Adv. Mater. 23, 3597-3602 (2011).

[39] P. Schilinsky, C. Waldauf, and C. J. Brabec, “Recombination and loss analysis in polythiophene based bulk heterojunction photodetectors,” Appl. Phys. Lett. 81, 3885-3887 (2002).

[40] D. W. Laird, S. Vaidya, S. Li, M. Mathai, B. Woodworth, E. Sheina, S. Williams, and T. Hammond, “Advances in Plexcore active layer technology systems for organic photovoltaics: roof-top and accelerated lifetime analysis of high performance organic photovoltaic cells,” Proc. SPIE 6656 Organic Photovoltaics VIII, 66560X (2007).

[41] K. M. Coakley, and M. D. McGehee, “Conjugated polymer photovoltaic cells,” Chem. Mater. 16(23), 4533-4542 (2004).

[42] H. Kallmann and M. Pope, “Photovoltaic effect in organic crystals,” J. Chem. Phys. 30, 585 (1959).

[43] B. R. Weinberger, M. Akhtar, S. C. Gau, "Polyacetylene Photovoltaic Devices," Synthetic Metals Vol. 4, Issue 3, 187–197 (1982).

[44] C. W. Tang, “Two-layer organic photovoltaic cell,” Appl. Phys. Lett. 48, 183-185 (1986).

[45] G. Yu, J. Gao, J. C. Hummelen, F. Wudl, A. J. Heeger, "Polymer photovoltaic cells: enhanced efficiencies via a network of internal donor-acceptor heterojunctions," Science 270, 1789 (1995).

[46] J. J. M. Halls, C. A. Walsh, N. C. Greenham, E. A. Marsegila, R. H. Friend, S. C. Moratti, and A. B. Holmes, "Efficient photodiodes from interpenetrating polymer networks," Nature 376, 498–500 (1995).

[47] M. C. Scharber and N. S. Sariciftci, "Efficiency of bulk-heterojunction organic solar cells," Prog. Polymer. Sci. 38 1929 (2013).

[48] N. S. Sariciftci, L. Smilowitz, A. J. Heeger, and F. Wudl, "Photoinduced electron transfer from a conducting polymer to buckminsterfullerene," Science 258(5087), 1474-1476 (1992).

[49] C. H. Lee, G. Yu, D. Moses, K. Pakbaz, C. Zhang, N. S. Sariciftci, A. J. Heeger and F. Wudl, "Sensitization of the photoconductivity of conducting polymers by C60: Photoinduced electron transfer," Phys. Rev. B 48, 15425-15433 (1993).

[50] H. Hoppe, M. Niggemann, C. Winder, J. Kraut, R. Hiesgen, A. Hinsch, D. Meissner, and N. S. Sariciftci, "Nanoscale morphology of conjugated polymer/fullerene based bulk-heterojunction solar cells," Adv. Funct. Mater. 14, 1005-1011 (2004).

[51] T. Martens, J. D'Haen, T. Munters, Z. Beelen, J. Manca, M. D'Olieslaeger, D. Vanderzande, L. De Schepper, and R. Andriessen, "Disclosure of the nanostructure of MDMO-PPV:PCBM bulk heterojunction organic solar cells by a combination of SPM and TEM," Synth. Met. 138, 243-247 (2003).

[52] V. D. Mihailetchi, J. K. J. van Duren, P. W. M. Blom, J. C. Hummelen, R. A. J. Janssen, J. M. Kroon, M. T. Rispens, W. J. H. Verhees, and M. M. Wienk, "Electron transport in a methanofullerene," Adv. Funct. Mater. 13, 43-46 (2003).

[53] S. E. Shaheen, C. J. Brabec, N. S. Sariciftci, F. Padinger, T. Fromherz, J. C. Hummelen, "2.5 % efficient organic plastic solar cells," Appl. Phys. Lett. 78, 841–843 (2001).

[54] J. K. J. van Duren, X. Yang, J. Loos, C. W. T. Bulle-Lieuwma, A. B. Sievel, J. C. Hummelen, and R. A. J. Janssen, "Relating the morphology of Poly(p-phenylene vinylene)/Methanofullerene blends to solar-cell performance," Adv. Func. Mater. 14, 425–434 (2004).

[55] V. D. Mihailetchi, L. J. A. Koster, P. W. M. Blom, C. Melzer, B. de Boer, J. K. K. van Duren, and R. A. J. Janssen, "Compositional dependence of the performance of

poly(p-phenylene vinylene):Methanofullerene bulk-heterojunction solar cells," Adv. Func. Mater. 15, 795–801 (2005).

[56] F. Padinger, R. S. Rittberger, and N. S. Sariciftci, "Effects of Postproduction Treatment on plastic solar cells," Adv. Func. Mater. 13,85–88 (2003).

[57] D. Chirvase, J. Parisi, J. C. Hummelen, and V. Dyakonov, "Influence of nanomorphology on the photovoltaic action of polymer-fullerene composites," Nanotechnology 15, 1317–1323 (2004).

[58] J. Huang, G. Li, Y. Yang, "Influence of composition and heat-treatment on the charge transport properties of poly(3-hexylthiophene) and [6,6]-phenyl C61-butyric acid methyl ester blends," Appl. Phys. Lett. 87, 112105 (2005).

[59] G. Li, V. Shrotriya, Y. Yao, Y. Yang, "Investigation of annealing effects and film thickness dependence of polymer solar cells based on poly(3-hexylthiophene)," J. Appl. Phys. 98, 043704 (2005).

[60] M. Reyes-Reyes, K. Kim, D. L. Carroll, "High-efficiency photovoltaic devices based on annealed poly(3-hexylthiophene) and 1-(3-methoxycarbonyl)-propyl-1-phenyl-(6,6)C61 blends," Appl. Phys. Lett. 87, 083506 (2005).

[61] T. Erb, U. Zhoukhavets, G. Gobsch, S. Raleva, B. Stühn, P. Schilinsky, C. Waldauf, and C. J. Brabec, “Correlation between structural and optical properties of composite polymer/fullerene films for organic solar cells,” Adv. Funct. Mater. 15(7), 1193-1196 (2005).

[62] Y. Zhao, G. Yuan, P. Roche and M. Leclerc, "A calorimetric study of the phase transitions in poly(3-hexylthiophene)," Polymer 36, 2211–2214 (1995).

[63] W. Ma, C. Yang, X. Gong, K. Lee, and A. J. Heeger, “Thermally stable, efficient polymer solar cells with nanoscale control of the interpenetrating network morphology,” Adv. Funct. Mat. 15, 1617-1622 (2005).

[64] G. Li, V. Shrotriya, J. Huang, Y. Yao, T. Moriarty, K. Emery and Y. Yang, "High-efficiency solution processable polymer photovoltaic cells by self-organization of polymer blends," Nat. Mater.4, 864–868 (2005).

[65] V. D. Mihailetchi, H. X. Xie, B. de Boer, L. M. Popescu, J. C. Hummelen, P. W. M. Blom, L. J. A. Koster, "Origin of the enhanced performance in poly(3-hexylthiophene):[6,6]-phenyl C61-butyric acid methyl ester solar cells upon slow drying of the active layer," Appl. Phys. Lett. 89, 012107 (2006).

[66] F.-C. Chen, C.-J. Ko, J.-L. Wu, W.-C. Chen, "Morphological study of P3HT:PCBM blend films prepared through solvent annealing for solar cell applications," Sol. Energy Mater. & Sol. Cells 94, 2426–2430 (2010).

[67] J. H. Park, J. S. Kim, J. H. Lee, W. H. Lee, K. Cho, "Effect of annealing solvent solubility on the performance of poly(3-hexylthiophene)/methanofullerene solar cells," J. Phys. Chem. C. 113(40), 17579–17584 (2009).

[68] G. Li, Y. Yao, H. Yang, V. Shrotriya, G. Yang, and Y. Yang, "Solvent annealing effect in polymer solar cells based on poly(3-hexylthiophene) and methanofullerenes," Adv. Func. Mater. 17, 1636–1644 (2007).

[69] J. You, L. Dou, K. Yoshimura, T. Kato, K. Ohya, T. Moriarty, K. Emery, C.-C. Chen, J. Gao, G. Li and Y. Yang, "A polymer tandem solar cell with 10.6% power conversion efficiency," Nat. Commun. 4, 1446 (2013).

[70] J. Zhao, Y. Li, G. Yang, K. Jiang, H. Lin. H. Ade, W. Ma and H. Yan, "Efficient organic solar cells processed from hydrocarbon solvents," Nat. Energy 1, 15027 (2016).

[71] B. Minnaert and P. Veelaert, "A proposal for typical artificial light sources for the characterization of indoor photovoltaic applications," Energies 7, 1500-1516 (2014).

[72] B. Azzopardi, C. J. M. Emmott, A. Urbina, F. C. Krebs, J. Mutale and J. Nelson, "Economic assessment of solar electricity production from organic-based photovoltaic modules in a domestic environment," Energy Environ. Sci. 4, 3741-3753 (2011).

[73] S. E. Shaheen, "Mechanisms of operation and degradation in solution processableorganic photovoltaics," in IEEE 45th Annual Inter. Reliability Phys. Symp., Phoenix, AZ (2007).

[74] J. Kalowekamo and E. Baker, "Estimating the manufacturing cost of purely organic solar cells," Solar Energy, vol.83, issue 8, pp.1224-1231, 2009.

[75] F.C. Krebs, "Encapsulation of polymer photovoltaic prototype," Solar Energy Materials and Solar Cells, vol.90, issue 20, pp.3633-3643, 2006.

[76] F.C. Krebs, J.E. Carle, N. Cruys-Bagger, M. Andersen, M.R. Lilliedal, M.A. Hammond, and S. Hvidt, "Lifetimes of organic photovoltaics: photochemistry, atmosphere effects and barrier layers in ITO-MEHPPV:PCBM-aluminium devices," Solar Energy Materials and Solar Cells, vol.86, pp.499-516, 2005.

[77] J. A. Hauch, P. Schilinsky, S. A. Choulis, R. Childers, M. Biele, and C. J. Brabec, "Flexible organic P3HT:PCBM bulk-heterojunction modules with more than 1 year outdoor lifetime," Sol. Energy Mater. Sol. Cells, 92, 727–731 (2008).

[78] D. Herr and L. Strine, “Permeability targets for thin film,” Solar Industry Magazine, vol. 5, no.1, pp.13-16, 2012.

[79] B. Viswanathan, V. R. Subramanian and J. S. Lee, Materials and processes for solar fuel production (Springer Science+Business Media, New York, 2014) p.31.

[80] M. Kempe, “Evaluation of encapsulation materilas for PV applications,” Photovoltaics International Journal, 9th Ed., pp.170-176, 2012.

[81] M. D. Kempe, “Ultraviolet light test and evaluation methods for encapsulats of photovoltaic modules,” Solar Energy Materials and Solar Cells., vol.94, pp. 246-253, 2010.

[82] J. A. Hauch, P. Schilinsky, S. A. Choulis, R. Childers, M. Biele, and C. J. Brabec, “Flexible organic P3HT:PCBM bulk-hetero- junction modules with more than 1 year outdoor lifetime,” Solar Energy Materials and Solar Cells, vol.92, pp.727–731, 2008.

[83] J. A. Hauch, P. Schilinsky, S. A. Choulis, S. Rajoelson, C. J. Brabec, “The impact of water vapor transmission rate on the lifetime of flexible polymer solar cells,” Applied Physics Letters, vol. 93, pp.103306, 2008.

[84] C. H. Peters, I. T. Sachs-Quintana, J. P. Kastrop, S. Beaupre, Mario Leclerc, and M. D. McGehee, “High efficiency polymer solar cells with long operating lifetimes,” Advanced Energy Materials, vol. 1, pp.491-494, 2011.

[85] G. Li, C.-W. Chu, V. Shrotriya, J. Huang, and Y. Yang, “Efficient inverted polymer solar cells,” Applied Physics Letters, vol. 83, pp.253503, 2006.

[86] T. Kuwabara, T. Nakayama, K. Uozumi, T. Yamaguchi, and K. Takahashi, “Highly durable inverted-type organic solar cell using amorphous titanium oxide as electron collection electrode inserted between ITO and organic layer,” Solar Energy Materials and Solar Cells, vol.92, pp.1476–1482, 2008.

[87] Z. He, C. Zhong, S. Su, M. Xu, H. Wu and Y. Cao, “Enhanced power-conversion efficiency in polymer solar cells using an inverted device structure,” Nature Photonics vol.6, pp.591-595, 2012.

[88] Y. Zhou et al., “A universial method to produce low-work function electrodes for organic electronics,” Science, vol. 336, pp.327-332, 2012.

[89] Y. Kim, H. Kim, S. Graham, A. Dyer, J. R. Reynolds, “Durable polyisobutylene edge sealants for organic electronics and electrochemical devices,” Solar Energy Materials and Solar Cells, vol.100, pp.120-125, 2012.

[90] R. Paetzold, A. Winnacker, D. Henseler, V. Cesari, and K. Heuser, “Permeation rate measurements by electrical analysis of calcium corrosion,” Review of Scientific Instruments, vol.74, no.12, pp.5147, 2003.

[91] Y. Kim, N. Kim, H. Kim, S. Graham, “The development of thin film barriers for encapsulating organic electrocnis,” Electronics Components and Technology Conference, 2011.

[92] M. D. Kempe, A. A. Dameron, T. J. Moricone, M. O. Reese, “Evaluation and modeling of edge-seal materials for photovoltaics applications,” 36th IEEE Photovoltaics Specialist Conference, 2010.